SMALL SATELLITE ATTITUDE CONTROL FOR TRACKING RESIDENT SPACE OBJECTS

Dylan Conway,[*] Richard Linares,[†] and John L. Crassidis[‡]

This paper addresses the attitude determination and control problem for the University at Buffalo's GLADOS mission. The main objective of the mission is to collect multi-band photometric data of resident space objects to improve space situational awareness. The team plans to use two optical payloads, a wide-field camera and a spectrometer, to achieve this goal. The attitude control system uses feedback from the wide-field camera in order to track targets and allow the collection of spectral data. The development of this novel approach which is suitable for low-cost small satellites is presented. A numerical simulation of a modeled mission including environmental disturbances, reaction wheel limitations, and sensor errors and delays is outlined. Results of this simulation are then presented. The ability of this approach to effectively track targets within the narrow field-of-view of the spectrometer is demonstrated.

INTRODUCTION

The U.S. Space Surveillance Network (SSN) currently tracks approximately 22,000 objects orbiting Earth that are on the order of 10 cm or larger.[1] The NASA Orbital Debris Program Office estimates the number of Earth orbiting objects between 1 and 10 cm to be around 500,000.[2] The major sources of this orbital debris are fragments of non-functional launch vehicles and man-made satellites. These objects pose a serious hazard to operational spacecraft which are relied heavily upon for both civilian and military applications. The well-known collision of an Iridium communication satellite with an inactive Russian Kosmos satellite created a large number of debris fragments, nearly 1800 of which are currently tracked by the SSN.[3] This event highlighted the importance of characterizing the debris environment and enforcing measures to reduce debris for the protection of space-based assets. The concept of Space Situational Awareness (SSA) incorporates the need to detect, characterize, and track resident space objects.

The United States Air Force has identified persistent space situational awareness (SSA) in its *Technology Horizons* document as a key focus area for development over the next two decades.[4] A comprehensive SSA program should allow timely response to hostile actions from uncooperative resident space objects (RSOs). This need places both spatial and temporal resolution re-

[*] Undergraduate Student, University at Buffalo, State University of New York, Department of Mechanical & Aerospace Engineering, Amherst, NY 14260-4400. Email: dtconway@buffalo.edu.
[†] Ph.D. Candidate, University at Buffalo, State University of New York, Department of Mechanical & Aerospace Engineering, Amherst, NY 14260-4400. Email: linares2@buffalo.edu.
[‡] Professor, University at Buffalo, State University of New York, Department of Mechanical & Aerospace Engineering, Amherst, NY 14260-4400. Email: johnc@buffalo.edu.

quirements on the estimated debris state. Measurements from optical and radar ground-based sensor distributed across the globe allow estimation of debris size and orbital path. These sensors have a restricted coverage of space and are limited by weather, time of day and time of year. Some also require operational facilities on foreign soil. Radar is further limited in range and fails to provide sufficient data on objects in geosynchronous (GEO) orbit. This orbital belt is an especially important region and is used extensively by communications and meteorological satellites. The GLADOS mission being developed by the University at Buffalo as part of the Air Force Research Laboratory (AFRL) University Nanosatellite Program has the primary objective of investigating the utility of a space-based platform for space surveillance on the nanosatellite form factor. The goal of the mission is to collect photometric data of RSOs, particularly in GEO, that can augment the current Space Surveillance Network (SSN).

Two major efforts have been made to capitalize on a space-based platform for SSA: the Space Based Space Surveillance (SBSS) space vehicle and the Midcourse Space Experiment (MSX). The MSX launched in 1996 and featured the Space Based Visible (SBV) sensor which provided full coverage of space. In its first two years of operation, the SBV sensor developed a catalog of 1,000 objects over 24,000 observations.[5] The SBSS space vehicle is the first of a planned constellation of satellites to expand coverage of the SSN. It carries a 30 centimeter telescope mounted on a gimbaled platform with the ability to image objects throughout GEO.[6] The 1,100 kilogram satellite was launched in September 2010 with a planned five and a half year mission lifetime at a cost of $823 million.[7] One advantage of a nanosatellite platform such as GLADOS would be to reduce the cost of space surveillance satellites making a larger constellation economically viable.

The SBV sensor featured a wide field of view (FOV) CCD and was able to capture multiple targets in GEO at a time. By pointing the camera in a fixed inertial direction so that stars appeared as point sources of light, an object in orbit would then be identified by the streak it made as it moved across the image plane. This method is known as sidereal tracking and was the primary technique used for data collection by the SBV sensor.[8] The inertial position of the target would then be determined based on the position and attitude of the SBV sensor, and the start and end locations of the streak in the image plane. From this information, orbital predictions could be made so that data collected on an RSO during one tracking event could be associated with data collected on the same RSO during another event. Since data collection time during sidereal tracking is limited by the camera FOV and the relative velocity between the target and sensor, accurate orbital predictions are difficult and the risk of incorrect associations can threaten RSO catalog data integrity. By making frequent observations of the same target, orbital predictions can be improved.[9] This complicates data collection scheduling of a single platform responsible for providing full space coverage and may therefore necessitate multiple platforms. The process is made more difficult by the possibility of RSOs performing orbital maneuvers which would require restarting the orbital prediction process. The GLADOS mission will be able to collect spectral data from an on-board spectrometer which could improve object correlation.

The collection of spectral data requires tracking an object within the FOV of a spectrometer. Unlike the sidereal tracking used by the SBV sensor, this requirement will necessitate the use of ephermis tracking in order to extend the data collection time. This method requires slewing the satellite to maintain the target in the sensor FOV. The proposed spectrometer to be used for GLADOS will have a narrow FOV on the order of 0.1^{o} to isolate individual targets. This presents a serious challenge to the attitude control system for a low cost nanosatellite. In addition to the spectrometer, GLADOS will fly a wide FOV CCD sensor that can provide visible light data on objects and background stars. While full star tracker functionality from this sensor may not be feasible, it can provide feedback for controlling the spectrometer pointing direction. The data collection process can proceed as follows. The satellite is commanded to point in an approximate

inertial direction like in sidereal tracking. Once a streak is detected on an image and is identified as an RSO of interest, emphermis tracking can begin. The pixel location of the target RSO at the start and end of a single CCD integration cycle can be used to compute the relative attitude error between the spectrometer boresight direction and the line-of-sight (LOS) vector to the target if the rotation between the CCD and spectrometer frame is known through previous calibration. This error can then be fed into a simple PD controller to bring the object into the spectrometer FOV for data collection. The object can be maintained in this FOV over the duration of an observation using the feedback provided by CCD images. Spectral data and segments of the images containing the object and bright stars can be downlinked to a ground station for processing.

The data collection process described can be broken down into two distinct segments: RSO acquisition and RSO tracking. The acquisition process is more straightforward and is similar to traditional approaches to attitude control like that taken by the SBV. The CCD must be pointed in a desired inertial direction that may contain RSOs of interest. This places an inertial attitude knowledge requirement of half the CCD FOV on GLADOS. Since this sensor has a wide FOV, 14^{o} degrees in the case of GLADOS, low-cost attitude sensors can be used. For the vision-based ephermis tracking the only concern is the relative attitude error between the LOS vector to the target and the spectrometer boresight. The target must be brought into and maintained within the spectrometer FOV over the duration of a data collection event. This places a relative attitude knowledge and control requirement of half the spectrometer FOV on GLADOS. This can be met using LOS measurements to the target from the CCD. By obtaining this additional functionality from the CCD, the cost and complexity of GLADOS can be reduced significantly. The RSO orbit can later be estimated on the ground running the time-stamped data of light sources in the images through a star matching algorithm along with the corresponding GLADOS position data.

This paper presents a preliminary analysis of the attitude determination and control techniques to be implemented on GLADOS. The equations governing the sensor platform dynamics are provided and a simple control algorithm is developed for relative attitude control during ephermis tracking. Error sources are identified and a means of simulating them is established. Simulation results for typical data collection events are provided.

OBJECT TRACKING

The primary objective of the GLADOS mission is to collect photometric data from glinting objects to assess the utility of a space based platform in improving space situational awareness. Research is currently being conducted into the extraction of information from photometric data on spacecraft size, material composition, attitude and shape.[10, 11] In particular, objects in geosynchronous (GEO) orbit will be targeted since a large number of satellites exist there and are out of range of ground based radar. The current configuration of the science system includes a wide-field camera and a spectrometer for the collection of the required data. By using three-line element (TLE) set data of a target in GEO and the current position of GLADOS as estimated by an on-board GPS unit with an orbit propagator, the line-of-sight (LOS) vector to the target in an inertial frame can be determined. Using inertial attitude sensors, GLADOS can be reoriented to point its wide-field camera in the direction of the target. Once the target is acquired in the FOV, the pointing error between the spectrometer boresight direction and the LOS vector can be determined and minimized by performing a slew maneuver. Reaction wheels will be used as the primary actuators for this maneuver. This tracking process is simulated using MATLAB software.

Given the position of GLADOS and the target in an inertial frame, the LOS vector to the target in that frame can be computed by

$$\bar{r}_{LOS} = \bar{r}_T - \bar{r}_G \tag{1}$$

From this initial LOS vector, GLADOS can then be reoriented to acquire the target in the 14° camera FOV. Since this requires a coarse 7° of attitude control accuracy as compared to the approximately 0.05° of attitude control accuracy for tracking with the spectrometer, the later process is the focus of this paper. Once the target is detected by the camera, a centroiding algorithm is run to determine the center pixel location of the target. This can be performed at the start and endpoint of the streak made across the image plane. The accuracy of this centroiding process is expected to be on the ordered of 0.5 pixels.[12] From this pixel location, angle measurements can be made to the target to determine the unit LOS vector in the camera reference frame:[13]

$${}^{C}\bar{r}_{LOS} = \frac{1}{\sqrt{f^2 + x^2 + y^2}} * \begin{bmatrix} -x \\ -y \\ f \end{bmatrix} \tag{2}$$

In this equation, x and y are the target's pixel location in the image frame and f is the focal length. Note that the camera boresight is assumed to be along the z direction of the image frame. If this direction is collinear with the spectrometer boresight, the Euler axis and angle for the rotation between both boresight directions and the measured LOS vector can be found:

$$\bar{e} = \left[{}^{C}\bar{r}_{LOS} X \right] \begin{bmatrix} 0 \\ 0 \\ 1 \end{bmatrix} = [e_1 \quad e_2 \quad e_3]^T \tag{3a}$$

$$\theta_e = \cos^{-1}\left({}^{C}\bar{r}_{LOS} \cdot \begin{bmatrix} 0 \\ 0 \\ 1 \end{bmatrix} \right) \tag{3b}$$

If the two boresight directions are not collinear, the LOS vector must be first mapped from the camera frame to the spectrometer frame. This mapping is done using an attitude matrix that is initially calibrated on the ground and can be recalibrated in flight. The LOS vector in the spectrometer frame is then simple to find:

$${}^{S}\bar{r}_{LOS} = A_{SC}\, {}^{C}\bar{r}_{LOS} \tag{4}$$

The error quaternion can then be computed from the Euler axis and Euler angle:

$$\delta\bar{q} = \begin{bmatrix} \delta\bar{Q} \\ \delta q_4 \end{bmatrix} = \begin{bmatrix} e_1 \sin(\frac{\theta_e}{2}) \\ e_2 \sin(\frac{\theta_e}{2}) \\ e_3 \sin(\frac{\theta_e}{2}) \\ \cos(\frac{\theta_e}{2}) \end{bmatrix} \tag{5}$$

Since only one LOS vector is being used to determine this error quaternion, only two-axis relative attitude knowledge can be achieved. Therefore the error quaternion represents the rotation between the body frame and a tracking frame. The tracking frame is defined as the frame with two axes that correspond to those used in the image plane and its third axis along the LOS vector to the target. Therefore the roll about the boresight direction is assumed to be zero. The angular velocity between the two frames can be computed from the quaternion and the time rate of change in the quaternion, given by

$$\bar{v} = \begin{bmatrix} 0 \\ \bar{\omega}_{C/T} \end{bmatrix} = 2C\frac{d}{dt}\left(\begin{bmatrix} q_4 \\ \delta\bar{q} \end{bmatrix}\right) \tag{6a}$$

$$C = \begin{bmatrix} q_4 & q_1 & q_2 & q_3 \\ -q_1 & q_4 & -q_3 & q_2 \\ -q_2 & q_3 & q_4 & -q_1 \\ -q_3 & -q_2 & q_1 & q_4 \end{bmatrix} \tag{6b}$$

This error quaternion and angular velocity is fed into a simple PD control law to compute a control torque on the satellite to be demanded from the reaction wheels:

$$\bar{u}_c = K_p\delta\bar{q} + K_d\bar{\omega}_{C/T} \tag{7}$$

This control torque, along with disturbance torque, alters the motion of the satellite body and its reaction wheels through

$$\bar{u}_c = -\dot{\bar{h}} \tag{8a}$$

$$J\dot{\bar{\omega}}_{C/I} = -[\bar{\omega}_{C/I}x](J\bar{\omega}_{C/I} + \bar{h}) - \dot{\bar{h}} + \bar{u} \tag{8b}$$

Here, J is the satellite inertia and $\bar{h}$ is the wheel momentum. These basic equations and associated error models can be used to simulate the tracking process that must occur during a glinting event.

SIMULATION

CCD Error Model

In order to verify pointing requirements for tracking control, a satellite and mission model was developed and a numerical simulation was completed. This was done using MATLAB software. First an orbital path is generated at discrete time steps for both GLADOS in low-Earth orbit (LEO) and a target in GEO. At each time step the true LOS vector is computed using Eq. (1). The LOS vector measurement is made using the camera and the noise associated with this measurement is considered using the CCD sensor model.[14] To simulate the measured LOS vector, Eq. (2) is altered to assume a focal length of one to produce a unit vector in the LOS direction. Zero mean Gaussian noise for the pixel location error is added to the unit LOS vector:

$$\tilde{b} = \bar{b} + \bar{w} \tag{9a}$$

$$\bar{w} \sim N(\bar{0}, \Omega) \tag{9b}$$

$$\Omega = E\{\bar{w}\bar{w}^T\} = \sigma^2(I_{3x3} - \bar{b}\bar{b}^T) \tag{9c}$$

Once the measured LOS vector is generated, Eq. (3a) and Eq. (3b) are used to find the Euler axis and angle.

Updates from the camera are not instantaneous. The streak endpoints correspond to the target location at the beginning and end of some finite integration time, Δt_{int}. There locations are then known only after the streak detection and centroiding algorithm is completed which takes some time, Δt_{comp}. The known data for a single frame is then $\delta\bar{q}(t_o)$ and $\delta\bar{q}(t_o + \Delta t_{int})$. The numerical derivative is taken and the relative angular velocity, $\bar{\omega}_{C/T}(t_o + \Delta t_{int})$, is found. The controller can then apply a control torque at $t = t_o + \Delta t_{int} + \Delta t_{comp}$.

Controller Model

For simplicity, the camera and spectrometer boresight are assumed to be collinear. Therefore Eq. (5) is used to compute the error quaternion without needing to map the LOS vector into the spectrometer frame. The single-step backward difference equation is used to compute the rate of change in the quaternion over one time step. Using the current value of the error quaternion and its numerical derivative, the angular velocity between the body frame and desired tracking frame is found using Eq. (6a) and Eq. (6b). The angular velocity and error quaternion are fed into the PD controller shown in Eq. (7). Alternatively, the controller could directly use the optical flow of the object in the image plane for feedback. This has been done for visual tracking of single feature points in robotics applications.[15] In this case, initially computing the error quaternion and rate simplifies the computation of the control torque on the satellite.

Gains are selected for this controller by using a single-axis approximation, $u = J\ddot{\theta}$, with a desired natural frequency of 0.3 rad/s and a damping ratio of 0.8. The natural frequency is selected to be below the update rate of the camera:

$$G = \frac{\theta(s)}{\tau(s)} = \frac{1}{Js^2} \quad , \quad G_c = K_p + K_d s \tag{10a}$$

$$G_{CLTF} = \frac{G G_c}{1 + G G_c} = \frac{K_p + K_d s}{Js^2 + K_p + K_d s} \tag{10b}$$

$$K_p = J\omega_n^2 \tag{10c}$$

$$K_d = 2J\zeta\omega_n \tag{10d}$$

Reaction Wheel Model

The computed torque value is sent to a reaction wheel model that attempts to emulate the performance of the MAI-101 wheels which are the current selection for the GLADOS mission. The wheels have a torque input range of ±0.625 mN-m which is sent in the form of an 8-bit word. The desired torque is therefore rounded to the nearest 0.005 m-Nm: the minimum torque resolution. The command torque in the simulation is also capped at the maximum torque of the wheels. The wheel momentum is continuously monitored and in the event that the wheels saturate at their maximum momentum capacity of +1 m-Nms, the torque value will not exceed zero. If the wheels reach −1 m-Nms, the torque value will be limited to zero or greater.

In order to account for the wheel imbalances, a model of the static and dynamic imbalances is used.[16] The wheel rotation rates, $[\omega_x\ \omega_y\ \omega_z]^T$, the static imbalance, $[S_x\ S_y\ S_z]^T$, the dynamic imbalance, $[D_x\ D_y\ D_z]^T$, a random phase for each wheel, $[\varphi_x\ \varphi_y\ \varphi_z]^T$, and the offset of the wheel axes from the center of mass, $\bar{R}_w$, are required. The static and dynamic imbalance values for the MAI-101 wheels are 1e-6 kg·m and 40e-9 kg·m^2. The offset from the center of mass is assumed to be 3 cm in each direction. The force and torque from the static imbalance is

$$\begin{aligned}\bar{F}_s = &\left(S_y\omega_y^2 \sin(\omega_y t + \varphi_y) + S_z\omega_z^2 \sin(\omega_z t + \varphi_z)\right)\hat{i} \\ &+\left(S_x\omega_x^2 \sin(\omega_x t + \varphi_x) + S_z\omega_z^2 \sin(\omega_z t + \varphi_z)\right)\hat{j} \\ &+\left(S_x\omega_x^2 \sin(\omega_x t + \varphi_x) + S_y\omega_y^2 \sin(\omega_y t + \varphi_y)\right)\hat{k}\end{aligned} \tag{11a}$$

$$\bar{u}_s = [\bar{R}_w \mathrm{x}]\bar{F}_s \tag{11b}$$

The dynamic imbalance is

$$\begin{aligned}\bar{u}_D = &\left(D_z\omega_z^2\sin(\omega_z t+\varphi_z) - D_y\omega_y^2\sin(\omega_y t+\varphi_y)\right)\hat{i}\\ &+\left(D_x\omega_x^2\sin(\omega_x t+\varphi_x) - D_z\omega_z^2\sin(\omega_z t+\varphi_z)\right)\hat{j}\\ &+\left(D_y\omega_y^2\sin(\omega_y t+\varphi_y) - D_x\omega_x^2\sin(\omega_x t+\varphi_x)\right)\hat{k}\end{aligned} \quad (12)$$

These disturbances result in a high frequency jitter in the satellite attitude with amplitude that is proportional to the square of the wheel speed. Therefore it will be important for GLADOS to minimize wheel speeds prior to data collection events by dumping momentum through the magnetorquer coils.

Environmental Disturbance Model

In addition to disturbance torques from the wheel imbalances, environmental torque is also considered. The primary disturbance source from the environment in LEO is expected to be from the aerodynamic torque.[17] This torque is modeled by considering the bus shape. The area of the six sides, A_i, the vector from the geometric center of each side to the center of mass, $\bar{r}_{c,i}$, and the normal vector directed away from the satellite for each side, $\hat{n}_i$ is fed into the model. At a given time step, the velocity vector in an inertial frame and the satellite attitude are also fed into the model. The normal component of each face is mapped into the inertial frame and the cosine of the angle between this vector and the unit velocity vector is found:

$$^I\hat{n}_i = A^{T\,B}\hat{n} \quad (13a)$$

$$\cos(\theta_i) = {}^I\hat{n}_i \cdot {}^I\hat{V} \quad (13b)$$

If the cosine is less than zero, the face is at least partially facing the direction of motion. The force and torque on this face are

$$\bar{F}_i = -\frac{1}{2}\rho C_D V^2\cos(\theta_i)\,A_i * {}^I\hat{V} \quad (13a)$$

$$\bar{u}_{aero,i} = [\bar{r}_{c,i}x]\,\bar{F}_i \quad (13b)$$

This is repeated for all six faces. A drag coefficient of 2 and atmospheric density of 5e-13 kg/m^3 is assumed.[18] The disturbance torque from the Earth's magnetic field is also considered in the simulation. A script computed the local magnetic field based on the current satellite position using the IGRF model. The torque is simply the cross product between the satellite residual dipole moment and the local field vector. [19] A small arbitrary dipole moment vector is assumed and did not significantly impact the results of the simulation.

Dynamic Update Model

At each time step, the total torque on the satellite (control, internal disturbance and environmental) is used to propagate the satellite dynamics using Eq. (8a) and Eq. (8b). Numerical integration is performed to update the new angular velocity relative to an inertial frame. The quaternion derivative is found using

$$\dot{\bar{q}} = \frac{1}{2}\Xi(\bar{q})\bar{\omega}_B \quad (14a)$$

$$\Xi(\bar{q}) = \begin{bmatrix} q_4 I_{3x3} + [\bar{\varrho}x] \\ -\bar{\varrho}^T \end{bmatrix} \quad (14b)$$

The time step selected for the simulation is 0.005 seconds. This time step allows for at least ten samples per wheel rotation in order to accurately capture the impact of the reaction wheel jitter. A camera integration time of 0.7 seconds and a streak endpoint computation time of 0.3 seconds are assumed. This results in the controller updating once every second. In addition, a one degree error is given to the alignment of each wheel in an arbitrary direction.

RESULTS

A likely orbital path for GLADOS and a target object trajectory in GEO is plotted in Figure 1. The green region represents a 6 minute segment of both orbital paths. The tracking simulation occurs during this segment as it is representative of a high-probability glint event.

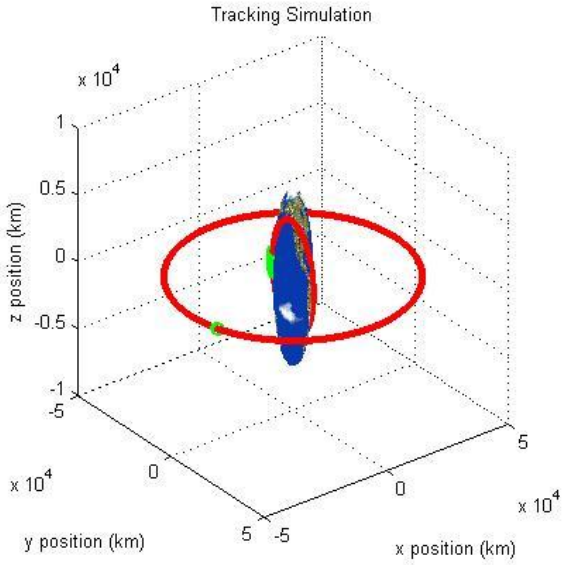

Figure 1: Typical orbital paths plotted in red. Tracking simulation occurs in the green region.

The primary objective as stated is to rotate the satellite so that the spectrometer boresight is pointed directly at the object. The target is initially acquired in the upper-right hand corner of the focal plane as seen in Figure 2. Over the course of three minutes, the target is brought to the center of the FOV and maintained there. The plot on the right is simply a zoomed in view of the target's pixel location. A one-sigma centroiding error value of 0.5 pixels which is equivalent to 11.3 arc-seconds for the camera being simulated is selected. The target is effectively maintained within a 6 ×6 pixel region.

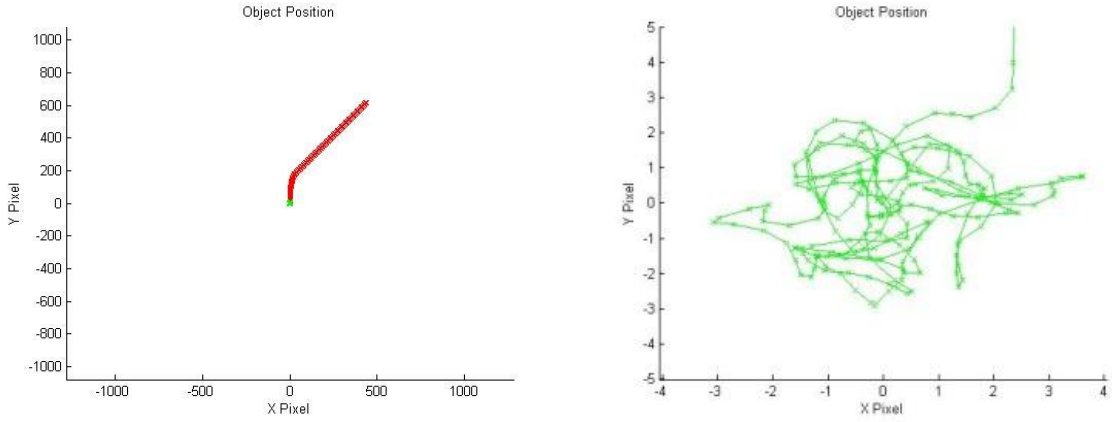

Figure 2: Target pixel location for an initial 5 degree pointing error.

The angular error versus time is plotted in Figure 3. The initial error of approximately six degrees is brought down to within the ±3 arc-minute limit represented by the red lines required for the spectrometer within 140 seconds. The error over the final three minutes has a mean of 1.3 arc-minutes with a standard deviation of 0.56 arc-minutes.

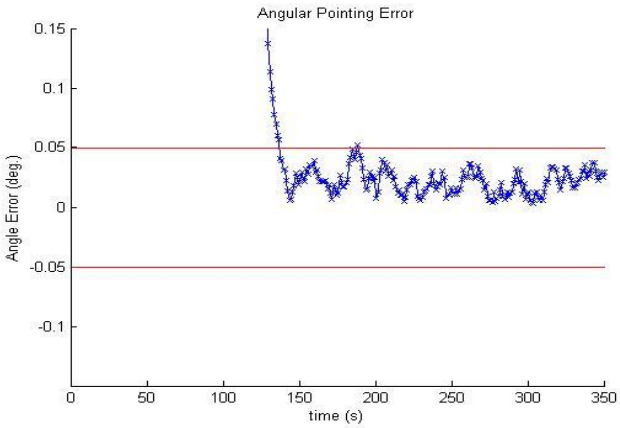

Figure 3: Angle error versus time.

The control effort provided by the reaction wheels to obtain this rotation is shown in Figure 4. The minimum torque resolution and the finite update rate are evident in the plots. The wheels are assumed to be spinning at 10% of their maximum speed when the tracking is initiated. Saturation of the wheels occurs over the first 5 to 10 seconds for the large initial angular error. As the target is brought to the center the control torque reverses directions and the momentum is reduced. These oscillations continue for steady state tracking.

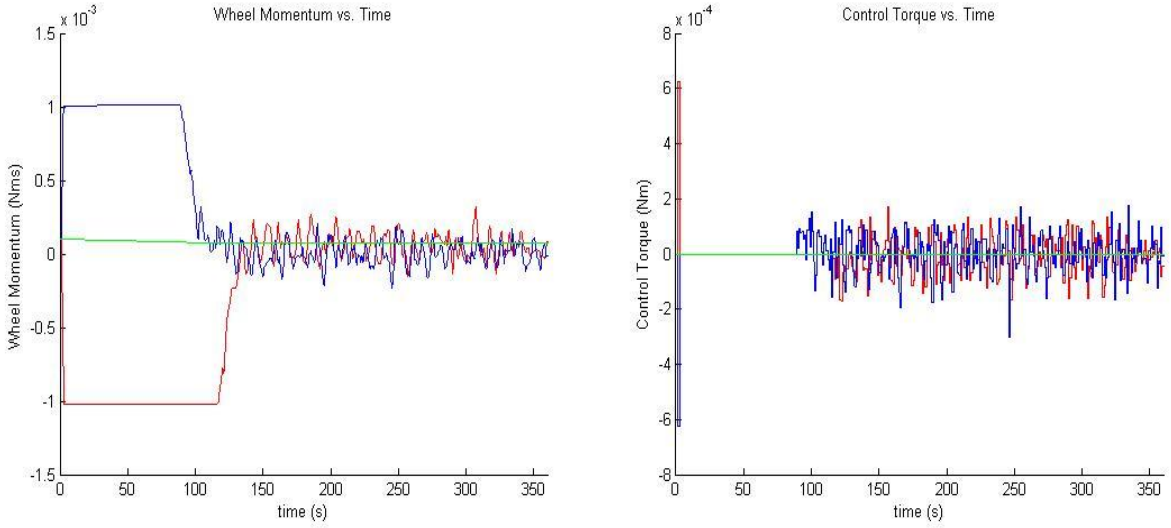

Figure 4: Control torque and wheel momentum for initial wheel speeds of +100 rpm.

The disturbance torque from the environment and reaction wheels is displayed in Figure 5. The total torque is dominated by the reaction wheel jitter which results in small high frequency

oscillations in the satellite attitude. The sinusoidal variation of the torque due to the imbalances is seen on the plot to the right. The initial high disturbance torque corresponds to the time period when the wheel speeds are greatest since the magnitude of the torque is related to the square of wheel speed. The impact of the environmental torque which is on the order of 10^{-8} Nm and changes slowly in time is minimal and only results in a small bias error in the pointing direction.

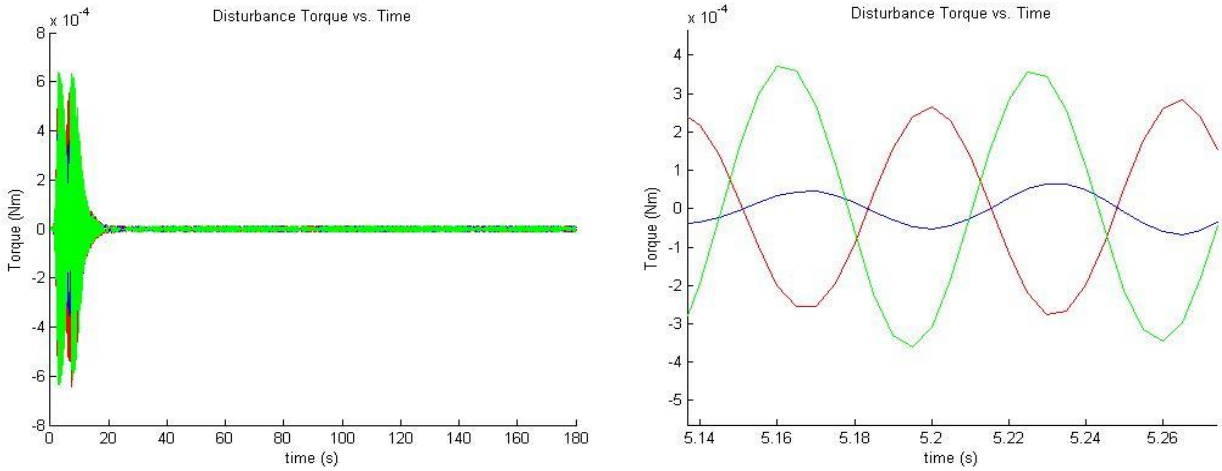

Figure 5: Total disturbance torque which is dominated by the reaction wheel jitter

The results of this simulation indicate that this algorithm is suitable for use on GLADOS. The data in Figure 2 and Figure 3 indicate the ability of this method to bring a target within the spectrometer FOV within two minutes and maintain it there continuously.

CONCLUSION

The algorithm used for attitude control in this case is unique in that only a single LOS vector from the camera is used for both attitude determination and control in ephermis tracking. No information from inertial attitude sensors or rate gyros is needed. The cross coupling term between axes, $-[\bar{\omega}_{C/I}x](J\bar{\omega}_{C/I} + \bar{h})$, often used as a feed-forward term in attitude control laws is neglected. Therefore uncertainty in the inertia properties does not significantly impact the pointing accuracy. For the simulated mission presented, neglecting this term was appropriate since the required angular velocity was relatively low. This also eliminates the need for high accuracy gyros and inertial sensors, which will significantly reduce the cost and complexity of the spacecraft. Only a low cost IMU to provide attitude estimates accurate to just half the CCD FOV is needed. However, the image processing required to detect target streak endpoints and to compute the LOS vector to these points will increase the computational load placed on the flight computer.

The simple and low-cost attitude control system presented could make a large constellation of small satellites economically feasible. This network of sensors could provide complete and continuous coverage of space for rapid responsiveness. Visible spectrum images from the CCD containing the target and background stars along with GPS data can be processed on the ground for orbit estimation. The spectrographic data collected by the network during each observation could solve issues relating to target correlation between observations. This is especially important for tracking operational spacecraft performing orbital maneuvers. In addition, the data may be able to provide attitude related information. The goal of the GLADOS mission is to demonstrate the potential for this technology in augmenting the current SSN.

ACKNOWLEDGMENTS

The authors would like to thank the Air Force Research Lab's sponsorship of the University Nanosatellite Program. This initiative has stimulated an array of design and research activities among students at many schools including the University at Buffalo. This paper is a direct result of those activities.

REFERENCES

[1]"Space Surveillance." *Air University*. US Air Force. Web. 12 Jan. 2012. <http://www.au.af.mil/au/awc/awcgate/usspc-fs/space.htm>.

[2]*NASA Orbital Debris Program Office*. Web. 12 Jan. 2012. <http://orbitaldebris.jsc.nasa.gov/index.html>.

[3]"Top Ten Satellite Breakups." *NASA Orbital Debris Program Office*. Orbital Debris Quarterly News, July 2010. Web. 2012.

[4]"Technology Horizons." United States Air Force, 15 May 2010. Web. 12 Jan. 2012.

[5]Lambour, R., R. Bergemann, C. Von Braun, and E. M. Gaposchkin. "Space-Based Visible Space Object Photometry: Initial Results." *Journal of Guidance, Control, and Dynamics* 23.1 (2000): 159-64.

[6]"Boeing: Space Based Space Surveillance (SBSS) System." *The Boeing Company*. Web. 12 Jan. 2012. <http://www.boeing.com/defense-space/space/satellite/sbss.html>.

[7]"Space Based Space Surveillance (SBSS)." *GlobalSecurity.org - Reliable Security Information*. Web. 12 Jan. 2012. <http://www.globalsecurity.org/space/systems/sbss.htm>.

[8]Gaposchkin, E. Michael, Curt Von Braun, and Jayant Sharma. "Space-Based Space Surveillance with the Space-Based Visible." *Journal of Guidance, Control, and Dynamics* 23.1 (2000): 148-52.

[9]Sharma, Jayant. "Space-Based Visible Space Surveillance Performance." *Journal of Guidance, Control, and Dynamics* 23.1 (2000): 153-58.

[10]Crassidis, John L. ""‘Astrometric and Photometric Data Fusion for Resident Space Object Orbit, Attitude, and Shape Determination’." Cornell, Ithaca. 29 Nov. 2011. Lecture.

[11]Jorgensen, Kira. *USING REFLECTANCE SPECTROSCOPY TO DETERMINE MATERIAL TYPE OF ORBITAL DEBRIS*. Thesis. University of Colorado, 2000. Print.

[12]Simms, L., V. Riot, W. De Vries, S. S. Olivier, A. Pertica, B. J. Bauman, D. Phillion, and Scott Nikolaev. *Optical Payload for the STARE Mission*. Tech. Livermore CA: Lawrence Livermore National Laboratory, 2011.

[13]Crassidis, John L., and John L. Junkins. *Optimal Estimation of Dynamic Systems*. Boca Raton, FL: Chapman & Hall, 2004. Print.

[14]Andrle, Michael S., Baro Hyun, John L. Crassidis, and Richard Linares. "Deterministic Relative Attitude Determination of Formation Flying Spacecraft." (2008). American Institute of Aeronautics and Astronautic. Web. 18 Dec. 2011. <http://www.acsu.buffalo.edu/~johnc/det_att08.pdf>.

[15]Papanikolopoulos, Nikolaos P., Pradeep K. Khosla, and Takeo Kanade. "Visual Tracking of a Moving Target by a Camera Mounted on a Robot: A Combination of Control and Vision." *IEEE TRANSACTIONS ON ROBOTICS AND AUTOMATION* 9.1 (1993): 14-35.

[16]Liu, Lulu. "Jitter and Basic Requirements of the Reaction Wheel Assembly in the Attitude Control System." *MIT* (2007). Web. 18 Dec. 2011. <http://web.mit.edu/lululiu/Public/TESS%20things/acs_analysis.pdf>.

[17]Wertz, James Richard., and Wiley J. Larson. *Space Mission Analysis and Design*. El Segundo, CA: Microcosm, 1999. Print.

[18]Stone, William C., and Christoph Witzgall. "Evaluation of Aerodynamic Drag and Torque for External Tanks in Low Earth Orbit." *Journal of Research of the National Institute of Standards and Technology* 111.2 (2006): 143-58.

[19]Svartveit, Kristian. "Attitude Determination of the NCUBE Satellite." *Department of Engineering Cybernetics* (2003).